Movement model of a human hand based on magnetic resonance imaging (MRI)

Georg Stillfried and Patrick van der Smagt

Abstract— Building on a long tradition of developing robotic hands, we are developing robotic systems closely copying human hands in its kinematic and dynamic properties. To this end, we require an exact computational model of human hand kinematics in order to obtain optimal grasping properties. From a large number of MRI recordings of hand bones in various grasps, we construct a parametrisable kinematic model, of which optimal versions can be determined. In this paper we present the required image processing and modelling methods as well as a resulting model.

Keywords: hand kinematics, finger joints, axes of rotation, MRI.

I. INTRODUCTION

Human hands are complex systems consisting of bones, joints, ligaments, tendons, muscles, fat and skin. In the course of evolution, they have developed a wide range of functionality. A human hand is able to perform precise tasks such as inserting a thread into a needle, and heavy-duty tasks like lifting a 20 kg load. This versatility has often attracted roboticists, who built robotic hands in varying degrees of anthropomorphism [1]–[4].

Robotic hands are applied as prostheses [5], [6], but could also be used in service robotics and telemanipulation. In all of these fields, copying the human movement will improve interaction with tools made for human hands, like keyboards and handles. In prostheses, human-like movement is also important for cosmetic aspects, while in telemanipulation, it facilitates a one-to-one mapping of human to robot movements.

Another field where an exact movement model is helpful is motion capturing, e.g. for analysing grasp movements. Motion capturing is commonly performed with an optical marker tracking system, e.g. Vicon [7]. If an exact model of the skeletal joints exists, joint angles can be computed from the optical measurements more precisely than when only the marker positions are used.

While the number of finger bones and the most important degrees of freedom are matched in some robotic hands, subtleties like inclined axes of rotation, palm arching and exact thumb motion are widely ignored. In order to allow for an intuitive use of robotic hands, these peculiarities should be known, and, as far as possible, implemented.

As far as we know, there are only few quantitative models of finger joints in literature [8]–[13]. None of these models

Georg Stillfried and Patrick van der Smagt are with the Institute of Robotics and Mechatronics, German Aerospace Centre (DLR). E-mail: {georg.stillfried, smagt}@dlr.de.
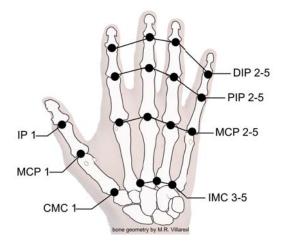
Fig. 1. Our model covers 18 joints: The carpometacarpal (CMC), metacarpophalangeal (MCP) and interphalangeal (IP) joint of the thumb, the intermetacarpal (IMC) joints of the palm and the metacarpophalangeal (MCP), proximal interphalangeal (PIP) and distal interphalangeal (DIP) joints of the fingers.

satisfy our requirements of an exact model of the entire hand, based on in-vivo measurements. The finger joints are commonly modelled as purely rotational joints with fixed axes, which seems a reasonable approximation (even though [12] models moving rotation axes).

In this paper we present a skeletal hand movement model that includes three joints of the thumb, three palm joints and three joints per finger (Fig. 1). The model is adjusted in such a way that it matches all of 50 live hand postures that were measured by magnetic resonance imaging (MRI). By measuring *in vivo* we make sure that the model reflects the *active* range of motion of the human hand.

Miyata et al. [12] presented a method similar to ours, but with a different objective: while we use 50 postures to build a continuous model of the finger bone trajectories, they used three postures and determined a separate helical axis for each posture. They also limited their analysis to the nine 1-DoF interphalangeal joints, while we consider 18 joints of the hand including the 2-DoF MCP and CMC joints.

II. METHODS

We build the model by recording hand postures, extracting and localising the bones, defining joint types and identifying joint parameters.

A. Data recording

Recording the kinematic movement of the human hand is not an easy thing to do. It must be taken into account that only *in vivo* recordings can be used to measure the effects described; after all, the behaviour of the soft tissue, tendons, and muscular structure greatly influence the kinematics of the hand.

Many methods have concentrated on observing the hand from the outside. As an example, Fioretti [14] used a camera system to observe the rotation of the index finger, in order to obtain data on the MCP bone. Other approaches have concentrated on visually measuring the joint angle of the fingers, or even used inaccurate devices such as DataGloves [15]. All of these methods, however, suffer from the problem that they do not use fixed reference points on the hand, but rather use a specific point on the skin as a stable reference point.

Even though the whole skin in itself, and especially the part of the finger tips with which the grasp is performed, is a key element in grasping, choosing any point on the skin gives a point of reference which changes during hand motion, and cannot be considered a stable point. All of the methods using markers on the hand are therefore rather imprecise; rather than measuring the motion of the whole finger, they measure the motion of one or more points on the skin, being subject to both active and passive influences.

In order to obtain a static reference point, we therefore investigate the movement of the *bones* in the hand, rather than any soft tissue reference point.

In order to simplify the recording of the hand movement, and due to the fact that we need *in vivo* measurements, we do not consider invasive methods to use the bones as markers. We rather use modern imaging methods to locate the hand and finger bones at the awake adult. Considering the high resolution that is required for these measurements, two viable approaches exist: (1) CT imaging and (2) MR imaging.

1) **CT imaging** (Computed Tomography) is a medical imaging method employing tomography where digital geometry processing is used to generate a three-dimensional image from a large number of two-dimensional X-ray images taken around a single axis of rotation. The nature of X-ray imaging makes it very well suited for bone imaging, and high-resolution 3D images can be obtained in a matter of seconds or minutes. However, CT relies on ionising radiation, which in high doses can cause cancer. Therefore, we exclude CT from our investigations.

2) **MR imaging** (Magnetic Resonance) has much greater soft tissue contrast than CT, without using ionising radiation. The scanner creates a powerful magnetic field which aligns the magnetisation of hydrogen atoms in the body. This causes the hydrogen atoms to emit a weak radio signal which is detected by the scanner and used to create a 3D image. Even though MR imaging is slower and results in lower resolution

Fig. 2. Hand inside a Philips SENSE head coil, which improves image quality on small body structures. The hand and the shown coil are inserted into the large MRI tube during the recording of the images.
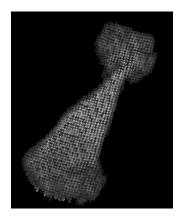

Fig. 3. A segmented voxel set of a bone. The brighter voxels in the inside of the bone reflect the high signal intensity emitted by the marrow, while the superficial layer (cortex) is shaded darker.

imaging, there are no health risks involved.

After several rounds of setting the correct parameters for the MR scanner, we do 4-minute steady 3D scans of the hand, with an isotropic resolution of $(0.76\,\text{mm})^3$ and an 8-bit intensity resolution per voxel. For image processing reasons we interpolate the images to a resolution of $(0.38\,\text{mm})^3$ per voxel. In order to both record the full hand, and obtain enough detail in the end phalanxes, we use a 8-channel Philips SENSE head coil (Fig. 2), leading to more homogeneous signals than when using the full-body coil integrated in the MR scanner. We record the data with a 1.5 T Philips Achieva scanner, using a balanced steady-state free precession (b-SSFP) sequence.

B. Finding the bones

After data recording we manually segment the bones in each of the images and store them separately using the 3D Dicom imaging tool Amira (Visage Imaging Inc., Andover, MA, USA). This manual preprocessing step leads to a set of segmented bones, each one being represented by a set of grey voxel values with 3D coordinates (Fig. 3).
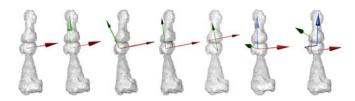
Fig. 4. The joint types considered in this paper. From left to right: 1-DoF; 1-DoF with two coupled axes of rotation; 2-DoF with freely oriented, intersecting axes; 2-DoF with mutually orthogonal, intersecting axes; 2-DoF with freely oriented, non-intersecting axes; 3-DoF with intersecting axes; 3-DoF with non-intersecting axes.

As a first step, we need to know the position and orientation of each bone in each MR image. We define one of the recorded hand posture as the reference posture. The position and orientation of a bone in another image is described as the translation and rotation that maps the bone from the reference image to the other image. We find this motion using a visual localisation approach described in [16]. It works by drawing point triples from both images and comparing point triples with similar edge lengths. The motion that is suitable to make most of these triangle pairs congruent is considered the best estimation for the motion of the bone from one image to the next.

Initial results show a very high uncertainty for the DIP joint of the index finger. It turns out that the distal phalanx of the index finger is often estimated to lie rotated about 180 degrees around its centre-line, when compared to its actual orientation. The reason for this is its nearly symmetrical shape. In order to avoid this error we use a modified version of the pose estimation algorithm that only allows rotation angles up to 120 degrees. Still, it turns out that the exact longitudinal orientation of the bones is quite difficult to measure.

Another step to improve pose estimation is to take only points close to the surface of the bones. This increases the probability that triangle pairs with similar edge length lie at the same position of the bone. We take a higher percentage of points for the small bones, in order to account for their higher surface-to-volume ratio.

C. Joint types

We consider joints with one, two and three degrees of freedom (DoF) with intersecting and non-intersecting axes. We use two versions of the two-DoF intersecting joint: one in which the axes are orthogonal to each other and another in which the axes are oriented freely. We define an additional joint type with one DoF and two coupled rotation axes, in which a flexion leads to a proportional longitudinal rotation of the bone. The joint types are shown in Fig. 4.

D. Identifying the joint parameters

For each joint, we calculate three sets of parameters:

1) The position of the centre of rotation (CoR),
2) the orientation of the axis of rotation (AoR),
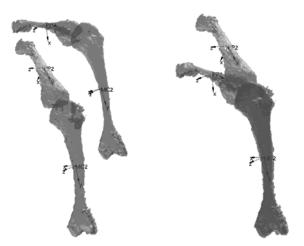3) the angular range of motion (RoM).

Fig. 5. Relative motion of a bone pair from the reference image to another image. On the left, the index finger metacarpal bone (MC 2) and proximal phalanx (PP 2) are shown in the positions and orientations in which they were measured in the reference image (left) and another image (middle). A transformation is applied to the bone pair in the other image, such that both measurements of the MC 2 bone coincide (right). The relative motion is then defined by the rotation and translation of the PP 2 bone from the reference image to the other image.

For the 1-DoF joint with two coupled axes we also calculate a coupling factor. In joints with two or three axes, we calculate two or three AoR orientations, as well as two or three CoR positions in the case of non-intersecting axes.

The basis for the calculation of the above parameters is the relative motion of the distal bone of a joint with respect to the proximal bone[1]. For this purpose we consider the proximal bone of the joint as fixed and the distal one as varying. In order to calculate the relative motion between the reference image and another image, we move the bone pair of the other image so that the proximal bones coincide (Fig. 5).

If we denote the pose estimations by the following homogeneous transformation matrices, $T_{\mathrm{P,ref}\to i}$ for the pose estimation of the proximal bone of image i (with respect to its counterpart in the reference image) and $T_{\mathrm{D,ref}\to i}$ for the pose estimation of the distal bone of image i, the relative motion $T_{\mathrm{Rel},i}$ is computed by

$$T_{\mathrm{Rel},i} = T_{\mathrm{P,ref}\to i}^{-1}\, T_{\mathrm{D,ref}\to i}. \qquad (1)$$

We compute the positions of the joint centres of rotation (CoRs) and the orientations of the joint axes of rotation (AoRs) by way of numerical optimisations, using the optimisation toolbox of the software package MATLAB (The Mathworks, Natick, MA, USA). For the CoRs we minimise the mean distance about which a point is displaced by the relative motions. This comes from the rationale that, in an ideal rotational joint, the CoR is at the same place before and after a movement of the joint.

For the AoRs, we minimise the mean twist between the modelled and measured orientations of the distal bone. The

[1]*Proximal* denotes structures that are closer to the body centre, *distal* denotes structures that are farther from the body centre.
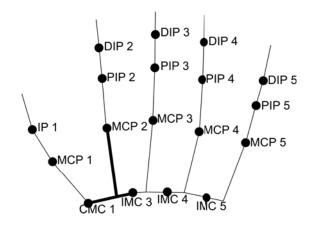
Fig. 6. The combination of joints into five kinematic chains. The thumb, index finger and middle finger chain start at the index finger metacarpal bone (thick line). The ring finger chain branches off from the middle middle finger chain at the IMC 4 joint. From there, the little finger chain branches off at the IMC 5 joint.

twist is defined as the rotation angle of an additional rotation that is needed to map the the modelled orientation onto the measured one. The optimisation of the AoR is in fact a nested optimisation consisting of an inner and and outer optimisation. The inner optimisation takes a given axis and finds the rotation angles that minimise the twist between the modelled and the the recorded orientations. The outer optimisation finds an axis orientation that results in the minimal *mean* twist.

We establish the RoM from the minima and maxima of the inner optimisation rotation angles, that is, the rotation angles that move the bone closest to its extreme positions.

E. Building the model

We select the joint types by setting a limit on the rotational and translational discrepancy between the modelled and measured bone poses and choosing the simplest joint type that fulfils the limit. For this, we consider joints with less DoF less complex than joints with more DoF, intersecting axes less complex than non-intersecting ones, and orthogonal axes less complex than freely oriented ones.

We model the hand as a set of five kinematic chains, one for each finger (Fig. 6). The chains lead from the basis of the index finger metacarpal, shown as thick black lines, to the respective fingertips. The joints are represented by black balls.

III. RESULTS

As a compromise between complexity and accuracy, we choose a limit of 6 degrees on the mean rotational error, and 3 mm on the mean translational error of each joint. The resulting joint types and their respective mean errors and ranges of motion are shown in Table I.

The whole hand model has 24 DoF, of which five are in the thumb, 16 in the fingers and three in the palm. The thumb CMC joint is a 2-DoF joint with non-intersecting axes, the thumb and finger MCP joints are 2-DoF joints with

TABLE I

<small>RESULTING JOINT TYPES AT A LIMIT OF 6 DEGREES AND 3 MM ON THE MEAN ERROR; RANGE OF MOTION; MEAN ROTATIONAL AND TRANSLATIONAL ERROR.</small>

joint name	joint type	axis no.	RoM (deg)	mean rot. err. (deg)	mean trans. error (mm)
CMC1	2-DoF with non-intersecting axes	1	68.7	3.6	2.6
		2	48.2		
MCP1	2-DoF with orthogonal intersecting axes	1	92.5	3	0.5
		2	49.0		
IP1	1-DoF		102.7	5.4	0.5
MCP2	2-DoF with orthogonal intersecting axes	1	110.2	3.4	0.6
		2	35.0		
PIP2	1-DoF		123.2	3.5	0.3
DIP2	1-DoF		101.1	4.3	0.4
IMC3	1-DoF		19.3	1.6	0.4
MCP3	2-DoF with orthogonal intersecting axes	1	117.8	2.1	0.5
		2	34.8		
PIP3	1-DoF		122.8	3.4	0.4
DIP3	1-DoF		106.5	4.5	0.4
IMC4	1-DoF		16.7	1.8	0.4
MCP4	2-DoF with orthogonal intersecting axes	1	126.5	3.4	0.7
		2	44.5		
PIP4	1-DoF		123.5	3.4	0.3
DIP4	1-DoF		104.8	3.9	0.3
IMC5	1-DoF		22.9	2.7	0.6
MCP5	2-DoF with orthogonal intersecting axes	1	51.0	2.5	0.5
		2	153.8		
PIP5	1-DoF		120.3	4.5	0.4
DIP5	1-DoF		103.6	4.5	0.3

orthogonal intersecting axes and the interphalangeal joints and palm joints are 1-DoF hinge joints.

Providing a proportional longitudinal rotation together with flexion did not yield a significant advantage in any joint. Also using freely oriented axes instead of orthogonal ones diminished the error only little or not at all. Joints with three DoF are only needed if the the limit on the mean rotational error is decreased to less than 5 degrees.

The range of motion is highest in the PIP joints with around 123 degrees, while the DIP joints exhibit a range of motion of 101 to 107 degrees. In the MCP joints, the flexion/extension range increases from the thumb (93 degrees) to the little finger (153 degrees), while the range of motion of the MCP abduction (sidewards) movement is between 35 and 51 degrees. The thumb CMC joint has a range of 69 degrees for flexion/circumduction and 48 degrees for ab-/adduction, and IMC joints move less than 23 degrees, each.

IV. DISCUSSION

Generally, using MRI turns out to be a viable method to precisely measure hand kinematics. Especially the mean translational error is low with 0.7 mm or less for all joints except the thumb CMC joint, where it is 2.6 mm. Possibly the movement of the *carpal* bones needs to be considered in future work in order to improve the thumb CMC joint
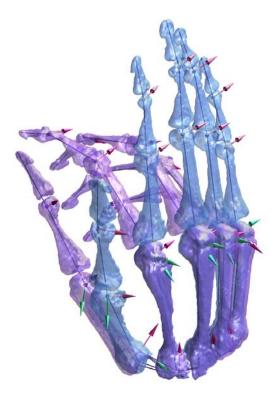
Fig. 7. The resulting hand model with 24 DoF, shown in two postures. The rotation axes are shown as arrows. The thumb CMC joint has two non-intersecting axes (bottom left). The MCP joints have two orthogonal, intersecting axes, with the first axis (red in the colour edition) responsible for flexion and extension in MCP 1-4 and for ab-/adduction in MCP 5. The IP, PIP, DIP and IMC joints have one axis of rotation, each.

accuracy. The longitudinal rotations of the bones are difficult to measure, which is reflected in the rotational accuracy of the model.

Only three of the seven joint types are used, but they fit well to the joint surface geometries: two non-intersecting axes matching the saddle shape of the CMC 1 joint surfaces, two orthogonal intersecting axes for the condyloid (egg-shaped) surfaces of the MCP joints and single axes for the cylindrically shaped interphalangeal joints. The movement of the intermetacarpal (palm) joints might actually be more complex than a hinge joint movement, but their small range of motion (less than 23 degrees) results in sufficiently small errors, even when the joint is modelled with only one axis.

It seems safe to use universal joints with orthogonal axes for MCP joints, and also the assumption of fixed rotational axes seems to be not too far from the biological movement (possibly excepting the thumb CMC joint). None of the joints exhibited a strong third degree of freedom, so that within the measurement accuracy, all joints can be taken as one- or two-DoF.

It must be kept in mind that this is a model of an individual hand. Applying the described procedure to data from a different subject will naturally yield a different kinematic model. Currently, we analyse data from two more hands to identify intra-individual similarities and differences in hand kinematics.

REFERENCES

[1] J. Butterfaß, M. Fischer, M. Grebenstein, S. Haidacher, and G. Hirzinger, "Design and experiences with DLR Hand II," in *Tenth International Symposium on Robotics with Applications (ISORA)*, June 2004.

[2] M. Grebenstein and P. van der Smagt, "Antagonism for a highly anthropomorphic hand-arm system," *Advanced Robotics*, vol. 22(1), pp. 39–55, 2008.

[3] H. Kawasaki, T. Komatsu, and K. Uchiyama, "Dexterous anthropomorphic robot hand with distributed tactile sensor: Gifu Hand II," *IEEE/ASME Transactions on Mechatronics*, vol. 7(3), pp. 296–303, 2002.

[4] L. Zollo, R. Stefano, E. Guiliemelli, M. C. Carrozza, and P. Dario, "Biomechatronic design and control of an anthropomorphic artificial hand for prosthetic and robotic applications," *IEEE/ASME Transactions on Mechatronics*, vol. 12(4), pp. 418–429, 2007.

[5] S. Adee, "Dean Kamen's "Luke Arm" prosthesis readies for clinical trials." Webpage: `http://spectrum.ieee.org/biomedical/bionics/dean-kamens-luke-arm-prosthesis-readies-for-clinical-trials`, February 2008. (Accessed on May 30, 2010).

[6] Otto Bock HealthCare GmbH, "Otto Bock - MyoHand VariPlus Speed." Webpage: `http://www.ottobock.com/cps/rde/xchg/ob_com_en/hs.xsl/19986.html`. (Accessed on May 30, 2010).

[7] OMG plc, "Motion capture systems from Vicon." Website: `http://www.vicon.com`. (Accessed on May 30, 2010).

[8] P. Cerveri, N. Lopomo, A. Pedotti, and G. Ferrigno, "Derivation of centers of rotation for wrist and fingers in a hand kinematic model: Methods and reliability results," *Annals of Biomedical Engineering*, vol. 33, pp. 402–412, 2005.

[9] A. Hollister, W. L. Buford, L. M. Myers, D. J. Giurintano, and A. Novick, "The axes of rotation of the thumb carpometacarpal joint," *Journal of Orthopaedic Research*, vol. 10, pp. 454–460, 1992.

[10] A. Hollister, D. J. Giurintano, W. L. Buford, L. M. Myers, and A. Novick, "The axes of rotation of the thumb interphalangeal and metacarpophalangeal joints," *Clinical Orthopaedics and Related Research*, vol. 320, pp. 188–193, 1995.

[11] X. Sancho-Bru, F. J. Valero-Cuevas, A. Pérez-González, D. J. Giurintano, M. Vergara-Monedero, and F. T. Sánchez-Marín, "Modeling the metacarpophalangeal joint in a biomechanical model of the index finger," in *Fifth International symposium on computer methods in Biomechanics and Biomedical Engineering*, (Rome), 2001.

[12] N. Miyata, M. Kouchi, M. Mochimaru, and T. Kurihaya, "Finger joint kinematics from MR images," in *IEEE/RSJ International Conference on Intelligent Robots and Systems*, 2005.

[13] L. Y. Chang and N. S. Pollard, "Method for determining kinematic parameters of the in vivo thumb carpometaracpal joint," *IEEE Transactions on Biomedical Engineering*, vol. 55(7), p. 1879ff, 2008.

[14] S. Fioretti, "Three-dimensional in-vivo kinematic analysis of finger movement," in *Advances in the Biomechanics of the Hand and Wrist* (F. Schuind, K. N. An, W. P. Cooney III, and M. Garcia-Elias, eds.), pp. 363–375, Plenum Press, 1994.

[15] M. Fischer, P. van der Smagt, and G. Hirzinger, "Learning techniques in a dataglove based telemanipulation system for the DLR hand," in *Transactions of the IEEE International Conference on Robotics and Automation*, pp. 1603–1608, 1998.

[16] U. Hillenbrand, "Consistent parameter clustering: definition and analysis," *Pattern Recognition Letters*, vol. 28, pp. 1112–1122, 2007.